A Reconfigurable Motor for Experimental Emulation of Stator Winding Inter-Turn and Broken Bar Faults in Polyphase Induction Machines

Chia-Chou Yeh[1], *Student Member, IEEE*, Gennadi Y. Sizov[1], *Student Member, IEEE*, Ahmed Sayed-Ahmed[1], *Student Member, IEEE*, Nabeel A. O. Demerdash[1], *Fellow, IEEE*, Richard J. Povinelli[1], *Senior Member, IEEE*, Edwin E. Yaz[1], *Senior Member, IEEE*, and Dan M. Ionel[2], *Senior Member, IEEE*

[1]Department of Electrical & Computer Engineering
Marquette University
Milwaukee, WI 53233, USA

[2]A. O. Smith Corporation
Corporate Technology Center
Milwaukee, WI 53224, USA

***Abstract* – The advantages and demerits of a 5-hp reconfigurable induction motor, which was designed for experimental emulation of stator winding inter-turn and broken rotor bar faults, are presented in this paper. It was perceived that this motor has the potential of quick and easy reconfiguration to produce the desired stator and rotor faults in a variety of different fault combinations. Accordingly, this would eliminate the need to permanently destroy machine components such as stator windings or rotor bars when acquiring data from a faulty machine for fault diagnostic purposes. Experimental results under healthy and various faulty conditions will be presented in this paper, including issues associated with rotor bar-end ring contact resistances, to demonstrate the benefits and drawbacks of this motor for acquiring large amounts of fault signature data.**

***Keywords* – Induction motor, fault diagnostics, condition monitoring, fault emulation, stator faults, broken bar faults, reconfigurable motors.**

I. INTRODUCTION

Polyphase induction motors have been the workhorse (main prime movers) for industrial and manufacturing processes as well as some propulsion applications. They are commonly used in ac adjustable speed drives where torque and speed control is indispensable. The ruggedness, ease of control, and cost-effective design of squirrel-cage induction motors are the main appealing features to consumers and engineers for the various above-mentioned applications. Due to its popularity, there have been many investigations on condition monitoring and fault diagnostics in electric machines throughout the literature, especially squirrel-cage induction motors [1]-[10]. This is because failure of such motors as prime movers can lead to significant undesirable repercussions such as production downtime, financial loss, adverse environmental effects, and possible personnel injury. Consequently, considerable interest in machine fault diagnostics received from industry and academia has prompted researchers to develop excellent state-of-the-art diagnostic techniques for various possible types of faults such as indicated in Fig. 1. The probability of occurrence of such faults is given in Table I, see [11],[12]. Therein, both the stator and rotor faults account for around 40 percent of all faults. Accordingly, the main thrust of this work centers on electrical stator and rotor faults.

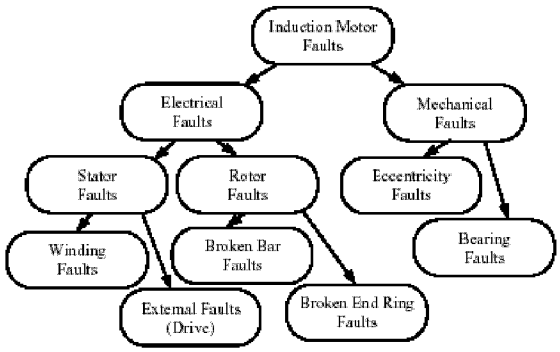

Fig. 1. Induction motor fault categories.

TABLE I
PERCENTAGE OF FAILURES BY MAJOR MOTOR COMPONENTS

Major Components	IEEE-IAS [11] % of Failures	EPRI [12] % of Failures
Bearing Related	44	41
Winding Related	26	36
Rotor Related	8	9
Other	22	14

In order to develop improved or novel stator and rotor fault diagnostic methods, extensive research has been done on the dynamic modeling of motor faults. This includes using the Time-Stepping Coupled Finite-Element State-Space technique to incorporate the stator and rotor faults for performance study and analysis [13]. It is desired to compare and verify these motor performances with physical data acquired from an actual motor with selected faults. Comparison between modeled and actual faults can significantly improve the fidelity of the simulation models and lead to improvements in future machine models representing various faulty conditions. Present methods of obtaining motor fault data are time

This paper is based upon work supported by the National Science Foundation under Grant No. ECS-0322974.

consuming and often require permanent deformation or destruction of motor components in order to perform the experiments. These actions of destruction of motor components are often irreversible and hence require several spare motors or their associated components in order to perform experiments of various fault scenarios. The machine components used for these tests are experiment specific and often require a significant amount of storage space. These costly obstacle could be overcome through the use of a reconfigurable induction motor which can physically and experimentally emulate such faults in a reversible manner that avoids permanent damage to motor parts. Accordingly, the design and testing of such a motor was the main thrust of this work.

The reconfigurable induction motor, which is the subject of this paper, is a 230/460-V, 60-Hz, 6-pole, 5-hp, squirrel-cage three-phase machine. This machine was built with a reconfigurable rotor and tested also with a production type aluminum die-cast squirrel-cage rotor. It possesses the advantages of quick and easy reconfiguration of the motor to produce the desired stator or rotor fault, or a combination of both. In addition, the utilization of the reconfigurable motor eliminates the need to permanently destroy machine components such as stator phase windings or rotor squirrel-cage bars. The thinking behind this effort was that having the versatility of the reconfigurable motor, large amounts of data can be acquired efficiently for analysis under a variety of different fault configurations or combinations. In this present phase of the work, the extent of the faults has been limited to stator winding inter-turn and broken bar faults due to their encompassing of around 40% of all motor faults, see Table I. Issues associated with the reconfigurable rotor cage design and resulting experimental data are fully detailed in this paper. The cast-type squirrel-cage was used to establish a healthy motor performance database of current and voltage waveforms, as well as Fast Fourier Transform (FFT) spectra [4],[5] and pendulous oscillation swing angle profiles [7]-[9].

This paper consists of three other sections. The first section is on the design concept and methodology of construction of the reconfigurable induction motor. The second section presents the experimental set-up, see Fig. 2, and test results obtained under normal operation using both the cast-type and reconfigurable squirrel-cages. This section also contains results of faulty operations for stator winding faults. In the same section, certain fault diagnostic techniques such as the pendulous oscillation phenomenon [7]-[9] and the negative sequence component concept [1]-[3] were utilized to diagnose the stator winding inter-turn faults using the experimentally acquired motor fault signature data. The purpose of such tasks is to verify the performance of the reconfigurable induction motor under healthy and faulty conditions. In addition, this section includes the rotor broken bar faults under load conditions and the diagnostic results using the FFT [4],[5] and pendulous oscillation [7]-[9] techniques, as well as the associated analysis of the reconfigurable squirrel-cage drawback issues. Finally, conclusions and recommendations are presented in the final section.

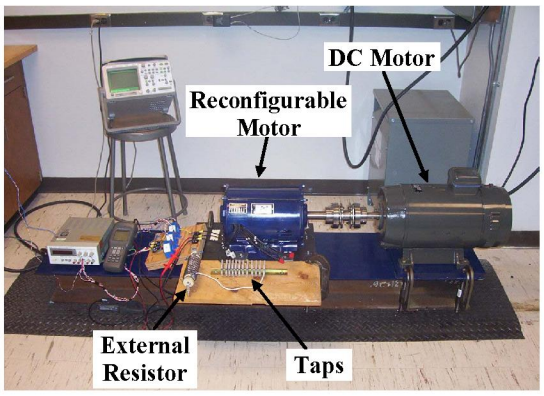

Fig. 2. Experimental Set-up.

II. The Reconfigurable Motor Design Concept and Methodology

The design of the reconfigurable motor was accomplished with the help of the frame size and configuration of an existing induction motor rated at 5-hp. In other words, the motor housing and the stator core of this existing 5-hp induction motor were used as the base design for the new reconfigurable induction motor. The remainder of the design consists of the rotor core, the rotor cage including the rotor bars and the end-rings, the shaft, the end cap which is used to secure the rotor bars into the end-rings, and the stator winding connections including winding taps to enable one to emulate a wide variety of stator short-circuit faults. The detailed design concepts of these reconfigurable motor components are given in the following sub-sections.

A. Stator Design

As mentioned earlier, the stator core was fabricated in such a manner so as to be identical to that of an existing 5-hp induction motor. The stator core consists of 36 slots, that is in this machine, there are 6 slots per pole (for a 6-pole motor) and 2 slots per pole per phase. A cross-sectional view of the motor is depicted in Fig. 3. To minimize the inherent cogging torque effects due to the space harmonics arising from the magnetic circuit geometric configurations and the effects of winding layouts the stator core was skewed by one slot pitch, that is by $30^{\circ}e$. The skewed stator including its winding coils is shown in Fig. 4. Meanwhile, the stator phase windings are double-layered, lap-connected with short pitched coils, each of a span of $150^{\circ}e$, see Fig. 5. The reason for skewing the stator and not skewing the rotor was to facilitate/ease the dismantling of the rotor cage bars when necessary, for rotor fault emulation purposes.

In order to emulate stator inter-turn short-circuit faults, the motor had a phase winding that was prepared with taps for purposes of "experimental mimicking" of incipient inter-turn faults. Ten taps were soldered sequentially every two turns, beginning with the "start" point of turn #1 and ending with the "start" point of turn #19 in only one phase of the machine, see the schematic winding diagram of Fig. 6. The limited number of taps to be soldered in the windings is restricted by the amount of space available inside the motor housing. These

taps are specially added at the motor terminal of one of the phases since the stator faults are likely to occur closest to the terminal end of the windings due to insulation stresses caused by the high switching effects from pulse-width modulated (PWM) drives [14]. To limit the short-circuit loop current, a variable external resistor was connected between the taps of the shorted portion of the winding turns, see Fig. 6. The design characteristics of this reconfigurable induction motor are given in Table II.

B. Rotor Design

A production type aluminum die-cast squirrel-cage, see Fig. 7, was prototyped for use with this motor to help collect a baseline healthy performance experimental database.

Previous efforts for emulating broken rotor bar faults have required different rotor bars to be broken by drilling out portions of such bars to physically break the continuity of the current conduction path through such bars. This process of emulating broken bar faults requires custom machining and the action (damage) performed on such rotors is irreversible. This method of bar breaking essentially limits the mix of combination and number of broken bars that can practically be made available for testing in a given motor, such as varying combinations of adjacent or non-adjacent bar breakages, which would necessitate a separate rotor for each desired set of broken bar configuration or scenario. A broken bar fault generally implies the presence of a nonconductive discontinuity (airgap) between the two broken bar sections. Therefore, this leads to the idea of constructing a reconfigurable rotor in which the rotor bars can be removed at will to emulate broken bar faults. The thinking was that the advantage of this reconfigurable rotor lies in its ability to create a large number of combinations of broken bar fault scenarios using the same rotor cage and the potential reversibility of such bar breakages.

The core was manufactured from the same type of steel laminations that were used to manufacture the stator core. As mentioned above, for the convenience of inserting the rotor bars into the lamination stack, the rotor core was not skewed. Again, in order to eliminate any cogging effect present in the motor torque due to space harmonic effects, the stator core, as mentioned above, was skewed by one stator slot pitch of $30^{\circ}e$. Since the rotor core was not skewed, the rotor bars were accordingly designed to have a layout parallel to the axis of rotation and they were fabricated from a copper alloy, see Figs. 8 and 9. The rotor end-rings were also made of the same material as the rotor bars, and the geometry of the end-rings were designed with an outer diameter equal to that of the rotor core. The design was conceived in such a manner that allows the end-rings to be removed and hence the rotor bars become easily accessible for removal or insertion from or into the rotor slots. Due to the fact that the rotor bars are not welded to the end-rings such as in typical motor designs, the slots of the end-rings were generously coated with conductive grease to ensure a good electrical conduction path to the bars. The rotor bars and the end-rings, as well as the complete rotor are depicted in Figs. 8 and 9, respectively. In this reconfigurable motor, there are a total of 46 rotor bars.

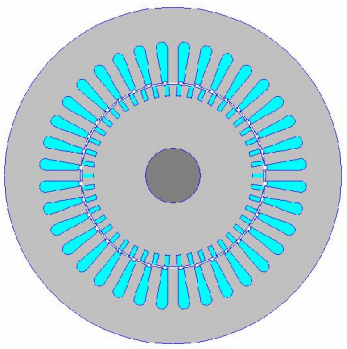

Fig. 3. Cross-sectional view of 5-hp reconfigurable motor.

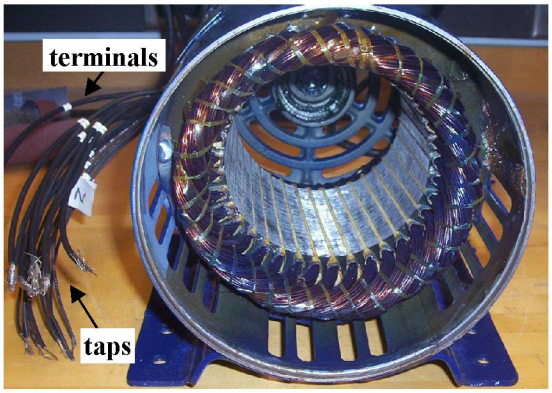

Fig. 4. Skewed stator with winding coils and taps.

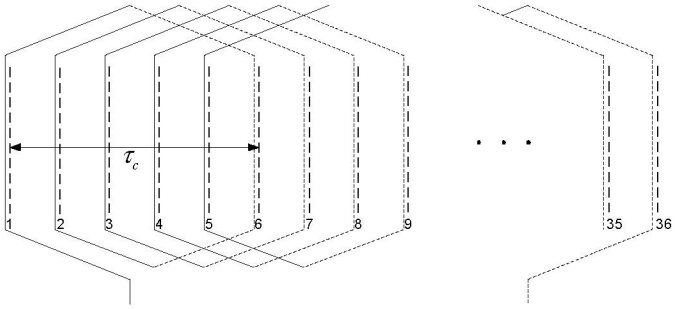

Fig. 5. Stator winding layouts with short pitched coils.

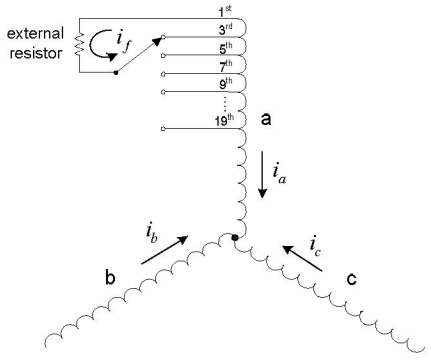

Fig. 6. Schematic diagram of stator windings with taps.

TABLE II
5-HP INDUCTION MOTOR CHARACTERISTICS

Power (hp)	5
Voltage (V)	230/460
Current (A)	16.2/8.1
Speed (r/min)	1150
Number of Poles	6
Number of Coils Per Phase	12
Number of Turns Per Coil	20
Number of Turns Per Phase	240
Type of Stator Windings	Double-Layer, Lap
Number of Stator Slots	36
Number of Rotor Bars	46
Number of Taps (in phase *a*)	10

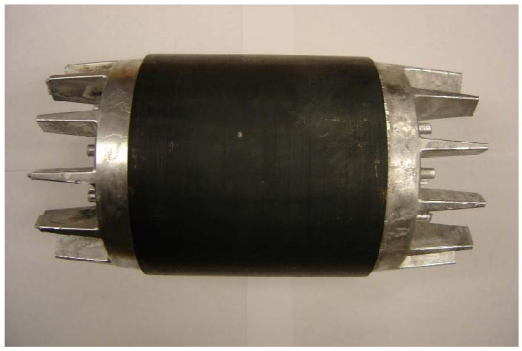

Fig. 7. Die-cast squirrel-cage.

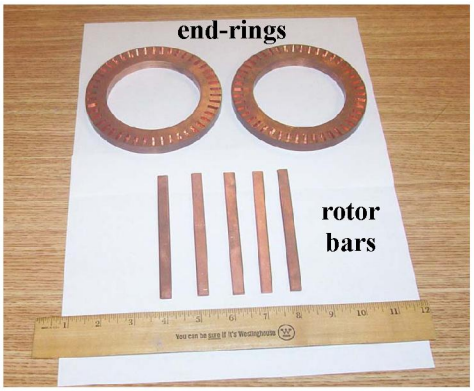

Fig. 8. Rotor bars and end-rings.

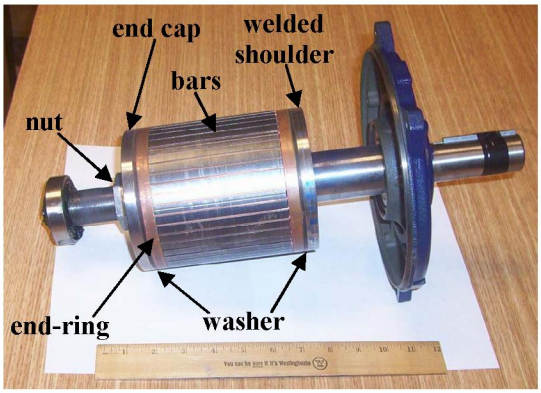

Fig. 9. Reconfigurable squirrel-cage rotor.

C. *Shaft and End Cap Design*

The shaft was constructed by machining a steel rod to its desired geometry. Two keyways, which were 180° from each other, were milled into the shaft to secure the rotor core. In a typical production induction motor of this size and rating, the rotor core, including the aluminum die-cast cage, is "hot dropped" on the shaft to form one inseparable assembly. This is not the case for the reconfigurable rotor at hand. Here, a custom shoulder was welded to the drive end of the shaft in order to secure the position of one of the end-rings. A nonconductive washer was added to act as an insulator between the shoulder and the end-ring, see Fig. 9. Meanwhile, opposite to the drive end of the shaft, in order to tighten the other end-ring to the rotor core, an end cap of the same diameter as the rotor was designed to slide down the shaft to secure that end-ring. Again, a nonconductive washer was added as an insulator between the end cap and that end-ring, see Fig. 9. Threads were added to the non-drive end of the shaft so that the end cap could be secured to the end-ring using a nut, see Fig. 9 for the details. Meanwhile, a keyway was inserted in the square slot formed by the rotor and the end cap to secure these parts to the shaft so that they rotate as one piece with the shaft.

III. EXPERIMENTAL RESULTS AND ANALYSIS

A. *The Healthy Motor Test Results*

The motor was tested at full load and rated frequency using the die-cast squirrel-cage rotor. It should be mentioned that the motor was energized from an open-loop (constant Volts/Hertz) commercially available PWM-inverter drive. The resulting FFT spectrum of its stator current waveform is given in Fig. 10, and its corresponding profile of the magnetic field pendulous oscillation [7]-[9] is given in Fig. 10. The lack of presence of any distinct lower side-band in the FFT spectrum of Fig. 10 indicates that there are no broken bars or anomalies present in this cage. The lack of a fundamental *2sf* component of pendulous oscillation angle in Fig. 11 confirms the lack of bar breakage or other squirrel-cage anomalies in this die-cast baseline case.

B. *Test Results of Stator Inter-Turn Shorts*

Test data were collected on stator inter-turn winding shorts using the reconfigurable rotor for this case of the subject 230/460-V, 6-pole, 5-hp, squirrel-cage induction motor fed from a commercially available PWM-inverter drive. The test was performed under open-loop (constant Volts/Hz) PWM control excitation fed from a 460-V utility supply. The stator inter-turn fault test data presented herein were obtained under healthy, two, six, ten, twelve, fourteen, and sixteen shorted turns at 50% load condition. The inter-turn short-circuit was achieved through an external resistor of 1Ω, see Fig. 6, in order to restrict the shorted loop current, i_f, to a safe level of current that does not cause permanent coil damage.

In order to verify the motor performance under inter-turn short circuit fault conditions, two fault diagnostic techniques, namely the pendulous oscillation phenomenon [7]-[9] and the

negative sequence component concept [1]-[3], were utilized. As reported in [9], the range of the pendulous oscillation (swing angle) progressively increases with an increase in the number of shorted turns, provided that the amplitude of the circulating loop (fault) current, I_f, exceeds the amplitude of the line current, I_a (or the positive sequence component of stator currents, I_p). This progressive increase in the swing angle magnitude, $\Delta\delta$, with the number of shorted turns (ST) can be observed in Fig. 12 and Table III. Notice in Fig. 12 that the swing angle, $\Delta\delta$, is plotted with respect to the circulating loop current ratio, I_f / I_a (or I_f / I_p). A similar trend can also be observed using the negative sequence component concept [1]-[3] as illustrated in Fig. 13 and Table III. Notice in Fig. 13 that the magnitude of the negative sequence component of stator currents, I_n, progressively increases with an increase in the number of shorted turns, if and only if the circulating loop current exceeds the line current. It is of importance to mention that the swing angle and the negative sequence current component are nonzero under a healthy condition due to the inherent motor manufacturing imperfections which resulted in slight unbalances in the motor phase *a*, *b*, and *c* currents. From these test results, one can conclude that the reconfigurable motor has the capability of emulating stator winding inter-turn faults.

C. Test Results of Reconfigurable Rotor Faults

In the reconfigurable squirrel-cage case, the rotor circuit did not yield consistent results when operated under healthy condition, that is with none of the rotor bars missing. The spectrum of the phase currents corresponding to this healthy case shows considerable side-bands, see Fig. 14.

A test was conducted involving electrically insulating one of the end-rings at the non-drive end of the rotor, with the motor being energized for starting purposes. Normally, one would expect zero starting torque and hence no rotation. However, it was observed that the motor exhibited a non-zero starting torque and the shaft began to turn as a result. This indicated to these investigators the presence of current loops in the cage that could have only resulted from circuit shorts between the rotor laminations and some of the bars. This may be the result of damage to the lamination insulation due to the repeated assembly and disassembly process performed on this reconfigurable cage. Such shorts lead to asymmetry in the rotor mmf waveforms and to the existence of a forward rotating component of mmf at *sf* frequency and a backward rotating component at *-sf* with respect to the rotor which is rotating forward at *(1-s)f*. The latter *-sf* component gives rise to the *(1-2s)f* component of current in the stator which is seen under a condition with all bars present in this rotor. This is in addition to the possible presence of bad conductive contacts between the bars and the end-rings resulting from the repeated disassembly and assembly process. Thus this leads to the appearance of conductive discontinuities in the rotor loop currents, and the appearance of effects that resemble the presence of broken bars. The use of conductive grease at the bar contact tips with the end-rings did not considerably improve the performance of the motor. The spectra of the motor phase currents corresponding to different fault scenarios of one, two and three broken bars, at full-load conditions are also depicted in Fig. 14. The fact that the side-band components did not follow the expected pattern of an increase in their magnitude with a corresponding increase in the number of broken bars can be attributed to the fact that the quality of the surface contact resistances between the end-rings and the bars could not be guaranteed in their consistency. Therefore, these contact resistances change from case to case because of the required disassembly of the rotor cage between the various tests. It was also found that the side-band components are highly dependent on the rotor cage temperature as illustrated for rotor cold and hot conditions in Fig. 15, which again tend to allude to the uneven distribution of contact resistances between the rotor bars and the end-rings.

The above results presented in current spectra form in Figs. 14 and 15 were reexamined using the pendulous oscillation method and the resulting pendulous oscillation fault indicators were consistent with our findings regarding inconsistencies in the contact resistances between bars and end-rings. These pendulous oscillation findings are given for the healthy and one through three missing "broken" bars in Fig. 16. Depicted in Fig. 17 is the time domain profile of the pendulous oscillation for the healthy rotor cage case. It is expected that the peak-to-peak value of the pendulous oscillation, also known as the swing-angle, in the healthy case should be negligible as shown earlier for the die-cast cage of Fig. 11. However, as can be seen from Fig. 17, this is not the case, meaning that there is a considerable distortion of the rotor magnetic field even in the healthy rotor cage case. These only result from conductive discontinuities in the cage circuit "masquerading" as bar breakages. As can be seen from the above results, both diagnostics techniques are in close agreement in so far as demonstrating the inadequacies of the reconfigurable rotor for broken bar fault emulation purposes.

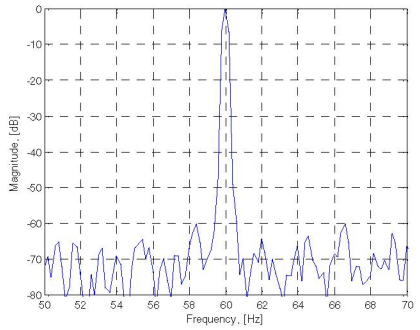

Fig. 10. Phase current FFT of healthy die-cast rotor cage.

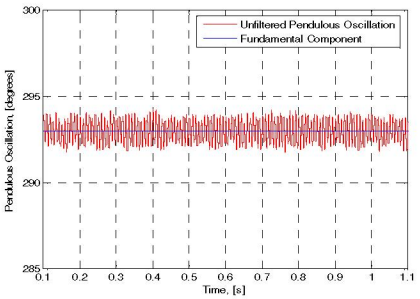

Fig. 11. Healthy die-cast rotor cage pendulous oscillation.

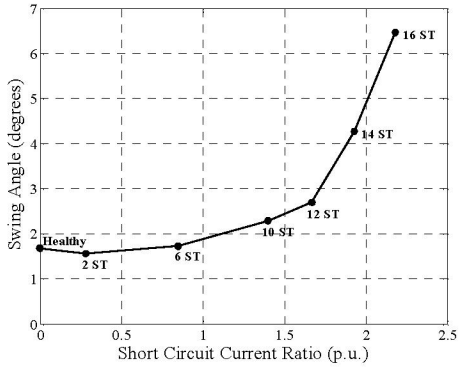

Fig. 12. The swing angle, $\Delta\delta$, versus the short circuit current ratio, I_f/I_p.

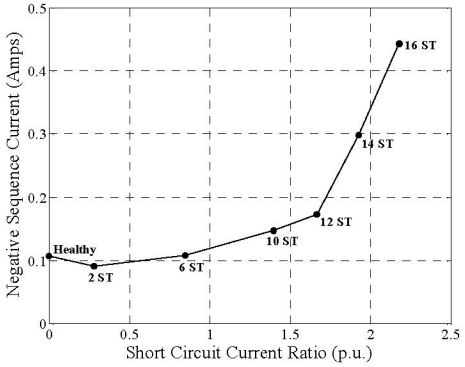

Fig. 13. The negative sequence current, I_n, versus the short circuit current ratio, I_f/I_p.

TABLE III
5-HP MOTOR DIAGNOSTIC RESULTS

ST	$\Delta\delta^\circ$	I_n(A)	I_p(A)	I_f(A)
0	1.689	0.107	9.011	0.000
2	1.574	0.091	8.996	2.566
6	1.732	0.108	9.040	7.697
10	2.302	0.147	9.157	12.829
12	2.703	0.173	9.225	15.394
14	4.286	0.298	9.298	17.960
16	6.478	0.443	9.411	20.526

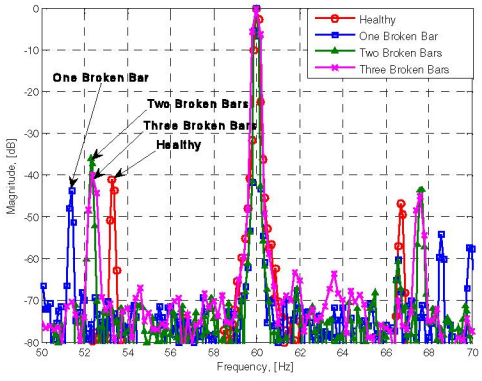

Fig. 14. Phase current FFT of healthy, one broken bar, two broken bars, and three broken bars.

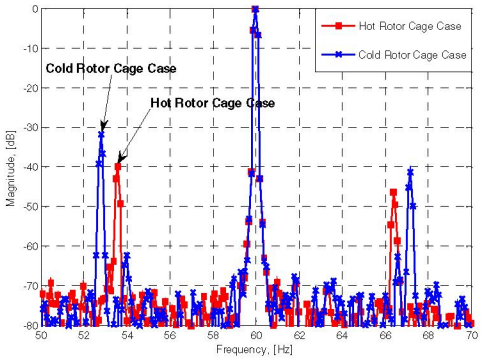

Fig. 15. Healthy rotor cage phase current FFT showing temperature dependence.

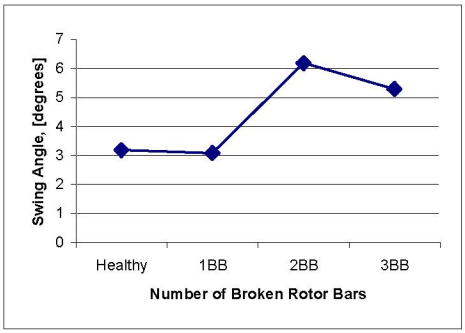

Fig. 16. Swing angle of healthy, one broken bar, two broken bars, and three broken bars.

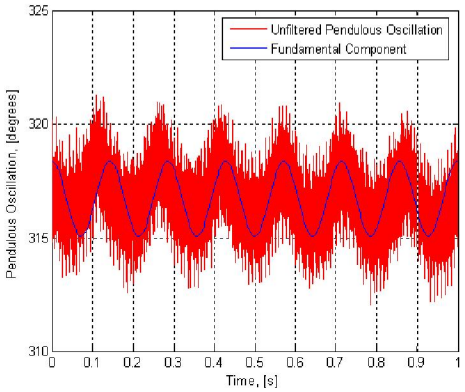

Fig. 17. Healthy rotor cage pendulous oscillation.

IV. CONCLUSIONS AND RECOMMENDATIONS

A 5-hp reconfigurable induction motor, which was designed for emulation of stator winding inter-turn and broken rotor bar faults, has been introduced. The experimental results obtained under stator inter-turn faults have demonstrated that the reconfigurable motor has successfully emulated stator inter-turn faults, which is further verified through the use of two diagnostic methods, namely the pendulous oscillation phenomenon and the negative sequence component concept. A complete set of test results, including a healthy rotor core using a die-cast rotor and rotor broken bar fault emulations using the reconfigurable rotor have been presented. It was found based on current spectrum side-band analysis and

magnetic field pendulous oscillation swing angle analysis that the electrical surface contacts between bars and end-rings in the reconfigurable cage and electrical shorts between bars and lamination material presented a problem that leads to the appearance of bar breakage indication where no such bar breakages are present. Hence, these authors are led to recommend that bars need hardened insulation coating to prevent lamination shorts, and highly improved conductive malleable material is needed for good electrical contact between bar ends and end-rings.

ACKNOWLEDGMENTS

The support of the A. O. Smith Corporation, which supplied and guided the manufacturing of the motor components is gratefully acknowledged, this is in addition to the support of the National Science Foundation under Grant No. ECS-0322974, which funded portions of this research.

REFERENCES

[1] G. B. Kliman, W. J. Premerlani, R. A. Koegl, and D. Hoeweler, "A New Approach to On-Line Turn Fault Detection in AC Motors," *Conference Proceedings in IEEE Industry Applications Annual Meeting*, Vol. 1, pp. 687-693, 1996.

[2] J. L. Kohler, J. Sottile, and F. C. Trutt, "Alternatives for Assessing the Electrical Integrity of Induction Motors," *IEEE Transactions on Industry Applications*, Vol. 28, pp. 1109-1117, Sep./Oct. 1992.

[3] R. M. Tallam, T. G. Habetler, and R. G. Harley, "Stator Winding Turn-Fault Detection for Closed-Loop Induction Motor Drives," *IEEE Transactions on Industry Applications*, Vol. 39, No. 3, pp. 720-724, May/Jun. 2003.

[4] A. Bellini, F. Filippetti, G. Franceschini, C. Tassoni, and G. B. Kliman, "Quantitative Evaluation of Induction Motor Broken Bars by Means of Electrical Signature Analysis," *IEEE Transactions on Industry Applications*, Vol. 37, pp. 1248-1255, Sep./Oct. 2001.

[5] N. M. Elkasabgy, A. R. Eastham, and G. E. Dawson, "Detection of Broken Bars in the Cage Rotor of an Induction Machine," *IEEE Transactions on Industry Applications*, Vol. 28, pp. 165-171, Jan./Feb. 1992.

[6] H. A. Toliyat, T. A. Lipo, "Transient Analysis of Cage Induction Machines Under Stator, Rotor Bar and End Ring Faults," *IEEE Transactions on Energy Conversion*, Vol. 10, pp. 241-247, June 1995.

[7] B. Mirafzal and N. A. O. Demerdash, "Induction Machine Broken-Bar Fault Diagnosis using the Rotor Magnetic Field Space-Vector Orientation," *IEEE Transactions on Industry Applications*, Vol. 40, No. 2, pp. 534-542, Mar./Apr. 2004.

[8] B. Mirafzal and N. A. O. Demerdash, "Effects of Load Magnitude on Diagnosing Broken Bar Faults in Induction Motors Using the Pendulous Oscillation of the Rotor Magnetic Field Orientation," *IEEE Transactions on Industry Applications*, May/Jun. 2005.

[9] B. Mirafzal and N. A. O. Demerdash, "On Innovation Methods of Induction Motor Inter-Turn and Broken-Bar Fault Diagnostics," *IEEE Transactions on Industry Applications*, Vol. 42, No. 2, March/April 2006.

[10] C.-C. Yeh, B. Mirafzal, R. J. Povinelli, and N. A. O. Demerdash, "A Condition Monitoring Vector Database Approach for Broken Bar Fault Diagnostics of Induction Machines," *Conference Proceedings in IEEE International Electric Machines and Drives Conference*, 2005, Vol. 1, pp. 29-34, May 2005.

[11] IEEE Committee Report, "Report of Large Motor Reliability Survey of Industrial and Commercial Installation, Part I and Part II," *IEEE Transactions on Industry Applications*, Vol. 21, pp. 853-872, Jul./Aug. 1985.

[12] P. F. Albrecht, J. C. Appiarius, and D. K. Sharma, "Assessment of the Reliability of Motors in Utility Applications-Updated," *IEEE Transactions on Energy Conversion*, Vol. 1, pp. 39-46, Dec. 1986.

[13] J. F. Bangura and N. A. O. Demerdash, "Diagnosis and Characterization of Effects of Broken Rotor Bars and Connectors in Squirrel-Cage Induction Motors by a Time-Stepping Coupled Finite Element-State Space Modeling Approach," *IEEE Transactions on Energy Conversion*, Vol. 14, pp. 1167-1176, Dec. 1999.

[14] N. A. O. Demerdash, "Electrical Transients and Surges in Power Systems and Devices," Marquette University (Class Notes), 2005.